Forensic Science International 286 (2018) 86–95

Contents lists available at ScienceDirect

Forensic Science International

journal homepage: www.elsevier.com/locate/forsciint

Impact sites representing potential bruising locations associated with bed falls in children

Raymond Dsouza[1], Gina Bertocci*

Injury Risk Assessment and Prevention (iRAP) Laboratory, Bioengineering Department, University of Louisville, KY, USA

ARTICLE INFO

Article history:
Received 25 May 2017
Received in revised form 15 December 2017
Accepted 18 February 2018
Available online xxx

Keywords:
Bruising
Biomechanics
Child abuse
Injury assessment
Force sensor
Anthropomorphic test device

ABSTRACT

Bruising can occur as a result of accidental or abusive trauma in children. Bruises are an early sign of child abuse and their locations on the body can be an effective delineator of abusive trauma. Since falls are often reported as false histories in abuse, the ability to predict potential bruising locations in falls could be valuable when attempting to differentiate between abuse and accident. In our study we used an anthropomorphic test device (ATD), a surrogate representing a 12 month old child, adapted with a custom developed force sensing skin to predict potential bruising locations during simulated bed falls. The sensing skin is made of custom resistive force sensors integrated into a conformable skin, adapted to fit the contours of the ATD. The sensing skin measured and displayed recorded force data on a computerized body image mapping system when sensors were activated. Simulated bed fall experiments were performed from two initial positions (FF – facing forward and FR – facing rearward) and two fall heights of 61 cm (24 in) and 91 cm (36 in) onto a padded carpet impact surface. Findings indicated potential bruising primarily in two planes of the ATD body. The majority of contact regions and greater forces were recorded in one plane, with fewer regions of contact and decreased force exhibited in an adjoining second plane. Additionally, no contact was recorded in the two planes opposite the impact planes. Differences in contact regions were observed for varying heights and initial position. Limitations of ATD biofidelity and soft tissue properties must be considered when interpreting these findings.

1. Introduction

Child abuse is the leading cause of trauma-related fatalities in children [1]. In 2015, 75% of child maltreatment fatalities occurred in children younger than age 3 [1]. The rate of child abuse and neglect victims has increased by 3.8% from 2011 (658,000) to 2015 (683,000) in the U.S., resulting in an estimated 1670 deaths in 2015 [1]. However, we cannot be certain of how many child abuse cases go undiagnosed, since 50–80% of fatal or near-fatal abuse cases have evidence of prior injuries [2,3]. Infants (less than 1-year of age) are the most vulnerable to abuse and have the highest rate of victimization at 24.2 per 1000 children when compared to all age groups [1].

While bruising can occur in accidental trauma, it is a common early sign of abuse in young children, especially those who are non-ambulatory [4]. Number, location, pattern and appearance of bruises have been shown to differ between abusive and accidental trauma [4–8]. The ability to differentiation between accident and abuse based upon bruising characteristics is critical in clinical and forensic settings, as this “roadmap” is indicative of a child's exposure to impact. Each bruise represents an impact and must be accounted for in the provided history to confirm compatibility between bruising patterns and stated cause. Determining compatibility is a critical part of the diagnostic and forensic assessment process, and can potentially prevent abused children from being returned to an unsafe environment where they may experience escalating or fatal abuse. Conversely, confirmation of compatibility could prevent innocent families from being wrongly accused of abuse.

The capability to predict potential bruising locations associated with common household falls which are often reported as false histories in child abuse does not exist and could prove useful in the

Abbreviations: ATD, anthropomorphic test device; FF, facing forward; FR, facing rearward; FF61, facing forward with a fall height of 61 cm (24 in); FF91, facing forward with a fall height of 91 cm (36 in); FR61, facing rearward with a fall height of 61 cm (24 in); FR91, facing rearward with a fall height of 91 cm (36 in); SBDS, surrogate bruising detection system; VI, virtual instrument; ANOVA, analysis of variance.

* Corresponding author at: Room 204 Health Sciences Research Tower, 500 S. Preston St, Louisville, KY 40202, USA.
E-mail addresses: raymond.dsouza@louisville.edu (R. Dsouza), g.bertocci@louisville.edu (G. Bertocci).
[1] Address: Room 110 Instructional Building B., 500 S. Preston St, Louisville, KY 40202, USA.

https://doi.org/10.1016/j.forsciint.2018.02.018
0379-0738/

Fig. 1. CRABI anthropomorphic test device (ATD) in side-lying, facing forward initial position for bed fall experiments. The pendulum actuator (providing the initial force to the posterior torso of the ATD to initiate the fall) is located behind the ATD.

distinction between abusive and accidental injuries. Thus, the goal of our study was to characterize potential bruising locations or patterns associated with a common childhood fall. In this study we used a bruising detection system to identify potential bruising patterns in simulated bed falls employing a child surrogate representative of a 12-month old child (stage of early independent mobility). The bruising detection system consisted of a pediatric anthropomorphic test device (ATD) equipped with a custom force sensing skin that is linked to display recorded force data on a computerized body mapping image system when the force sensors are activated [9]. Our intent was to document a "roadmap" of the surrogate's contact exposure during bed falls and to identify whether variations in fall parameters (fall height and initial position) led to differences in impact locations or patterns.

2. Methods

The surrogate bruising detection system (SBDS), consisting of the 12 month old CRABI ATD (10 kg mass) fitted with a force sensing skin and associated data acquisition hardware and analysis software, was used to predict potential bruising patterns in simulated fall scenarios. The sensing skin of the SBDS consists of 132 force sensors enveloping the surface of the ATD that is divided into seven regions including the head, anterior torso, posterior torso, forearm, upper arm, thigh and shank. Each region has individualized custom sensor arrays. Graphical programming software[2] was used to acquire and display sensor output in a manner that relates sensor location to body region. Additional details of the SBDS and its individual components are described in earlier publications [9,10].

The SBDS was used to assess potential bruising locations on the body during a series of bed fall experiments as this type of furniture fall is commonly experienced by young children.

Table 1
ATD initial joint angles.

Joint	Angle (degrees)
Right shoulder extension	135°
Right elbow extension	110°
Left shoulder extension	0°
Left elbow extension	170°
Hip (both) flexion	50°
Knee flexion	80°

2.1. Test setup

The ATD was placed in a side-lying position on the edge of a horizontal surface representing a couch or bed (Fig. 1). A swinging pendulum actuator supported by a tripod with a manually operated release mechanism was positioned at the ATD posterior mid-torso (approximate center of mass). The pendulum actuator consisted of a weight (2.5 kg) that was released (by a manually operated release mechanism) from its raised position (angle of 30° to the vertical) such that the weight made contact with the same location on the ATD torso. The pendulum actuator provided a consistent initial force sufficient to initiate roll of the ATD from the bed surface and fall freely under the effects of gravity. Fall experiments were conducted using two different initial conditions and two different bed heights. The impact surface for all the falls was padded carpet over a wooden subfloor.

Prior to each fall, ATD joint angles were adjusted using a goniometer to ensure repeated positioning in all tests (Table 1). Additionally, joint stiffness was calibrated to manufacturer specifications whereby the joints were tightened until the friction was just sufficient to support the weight of the limb against gravity. The impact surface evaluated for all fall scenarios was padded carpet over a wooden subfloor. The carpet surface consisted of a 1.3 cm (1/2 in) thick open loop carpet placed over 1.0 cm (3/8 in) thick foam padding. The carpet and padding were placed over a 1.9 cm (3/4 in) thick plywood platform 183 cm × 91.5 cm (6 ft × 3 ft) built to standard building codes with 5.1 cm × 10.2 cm (2 in × 4 in) joists, spaced 40.6 cm (16 in) on center.

2.2. Data acquisition and analysis

The SBDS's sensors consist of force sensing resistors whose outputs were fed to the data acquisition system through a voltage divider circuit to convert resistance to voltage. Data acquisition hardware[3] was used to capture and convert the analog sensor output. Multifunctional input/output data acquisition cards[4] (Resolution – 16 bit, Sample rate – 250 kS/s) acquired, conditioned and digitized the sensor output signals. The National Instruments PCI-6225 data acquisition card is capable of measuring 80 single ended analog channels at a 16 bit resolution and a sample rate of 250 kS/s. A personal computer served as the platform for the data acquisition hardware.

Graphical programming software[5] was used to acquire and display sensor output in a manner that relates sensor location to body region. A Virtual Instrument (VI) was developed to accomplish this objective. An active 3D (3-dimensional) body map image representing the ATD served as a graphical interface and was developed using Labview (National Instruments) software. The body image was discretely mapped to the sensors on the ATD such that active sensor outputs (those which have been

[2] Labview 2010; National Instruments, Austin, TX, USA.

[3] National Instruments, TX, USA.
[4] PCI – 6225; National Instruments, TX, USA.
[5] Labview 2010; National Instruments, TX, USA.

Table 2
Evaluated bed fall scenarios: fall height, ATD initial position and impact surface.

Fall height (in/cm)	Initial position	Surface type
61 cm (24 in)	**F**acing **F**orward(**FF**)	Carpet over wood
61 cm (24 in)	**F**acing **R**earward(**FR**)	
91 cm (36 in)	**F**acing **F**orward(**FF**)	
91 cm (36 in)	**F**acing **R**earward(**FR**)	

impacted) and their locations were displayed on the computerized body map image. Sensor outputs in terms of force magnitude were color-coded, designating a pre-determined force range so as to aid in the quick overview of locations with high intensities of impact. A personal computer served as the platform for the data acquisition hardware. A threshold force of 4.5 N (≈1 lb or 5% of ATD body weight) was used to establish the onset of contact between the ATD and impact surface.

Five trials of each simulated bed fall scenario (forward facing and rearward facing positions for both fall heights) were conducted onto carpet (Table 2) for a total of 20 fall experiments.

2.3. Motion capture

All falls were captured using a digital video camera (120 frames per second) to record overall fall dynamics. The camera was positioned so that the line of sight was perpendicular to the ATD sagittal plane. This allowed for qualitative assessment of fall dynamics.

2.4. Statistical analysis

A two-way analysis of variance (ANOVA) test was used to determine if changes in initial position and fall height led to significant differences in impact forces applied to body regions. Additionally, post hoc tests were conducted to further examine where significant differences existed ($p \leq 0.05$). Data was evaluated for normal distribution. Individual sensors were grouped by body region. Body regions were defined as head, anterior torso, posterior torso, left and right upper arm, left and right lower arm, left and right upper leg, and left and right lower leg.

3. Results

3.1. Fall dynamics and impact regions

All fall scenarios indicated potential for bruising in two planes with impact location primarily on the frontal, temporal and parietal head regions, anterior and posterior torso, and upper arm and upper leg regions.

3.1.1. Facing forward – 61 cm bed height (FF61)

The ATD initial position was forward facing (FF) such that the longitudinal (mid-sagittal plane) axis of the body was parallel with the floor (10 ms Fig. 2). Subsequent to actuator-ATD contact, the ATD rolled forward longitudinally about the edge of the bed surface (500 ms, Fig. 2). During free fall to the floor, the ATD continued to rotate about its longitudinal axis with the head surpassing the feet just prior to impact (750 ms, Fig. 2). The ATD impacted the floor on its left side with the left shoulder (the upper arm was impinged between the chest and floor) and left parietal region of the head impacting at approximately the same time (790 ms, Fig. 2). Following initial impact with the floor, the ATD rebounded upward from the floor before coming to rest (1000 ms, Fig. 2).

The SBDS body map image, showing four views (anterior, posterior, left lateral and right lateral), illustrates the ATD to floor surface impact locations (Fig. 3) for the FF61 bed fall (Fig. 2). Since the initial impact event was of primary concern, data associated with the secondary impact following rebound was not evaluated.

3.1.2. Facing forward – 91 cm bed height (FF91)

The initial ATD position was facing forward (FF) such that the longitudinal (mid-sagittal plane) axis of the body was parallel with the floor (10 ms, Fig. 4). Subsequent to actuator-ATD contact, the ATD rolled longitudinally forward about the edge of the bed surface (500 ms, Fig. 4). During the free fall to the floor, the ATD continued to rotate about its longitudinal axis with the head surpassing the feet just prior to impact (850 ms, Fig. 4). The ATD impacted the floor surface on its posterior side with the left posterior shoulder and parietal region of the head at approximately the same time (875 ms, Fig. 4). Following the initial impact with the floor, the ATD rebounded upward off the floor before coming to rest (1000 ms, Fig. 4).

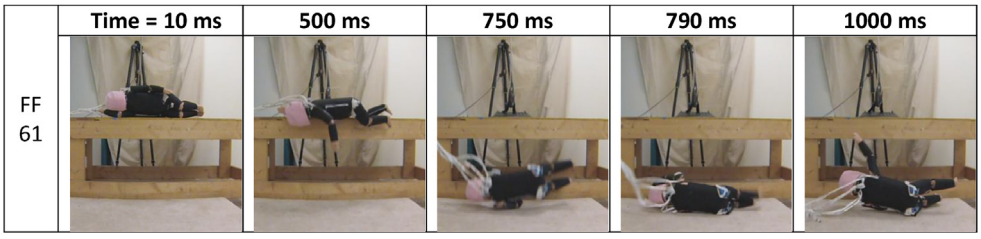

Fig. 2. Video frame sequences showing FF61 (24 in) bed fall onto the padded carpet surface at corresponding time intervals.

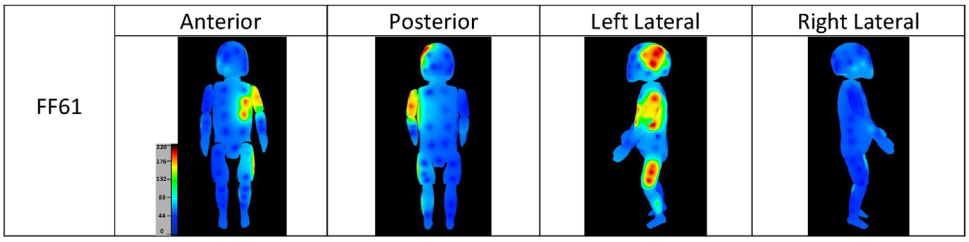

Fig. 3. Representative SBDS body map image corresponding to FF61 (24 in) bed fall illustrating body regions of impact. Color and intensity vary depending on the level of force imparted to specific regions during the fall event. (For interpretation of the references to color in this figure legend, the reader is referred to the web version of the article.)

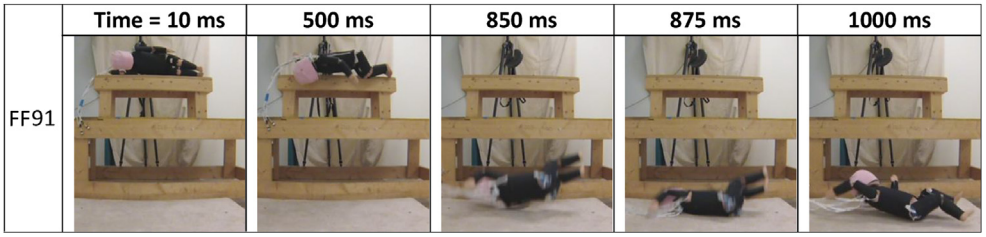

Fig. 4. Video frame sequences showing FF91 (36 in) bed fall onto padded carpet surface at corresponding time intervals.

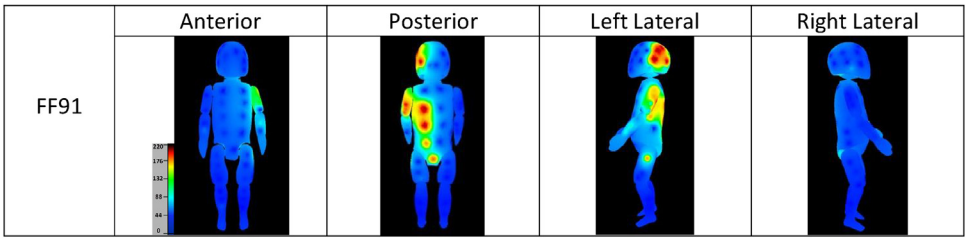

Fig. 5. Representative SBDS body map image corresponding to FF91 (36 in) bed fall illustrating body regions of impact. Color and intensity vary depending on level of force imparted to specific regions during the fall event. (For interpretation of the references to color in this figure legend, the reader is referred to the web version of the article.)

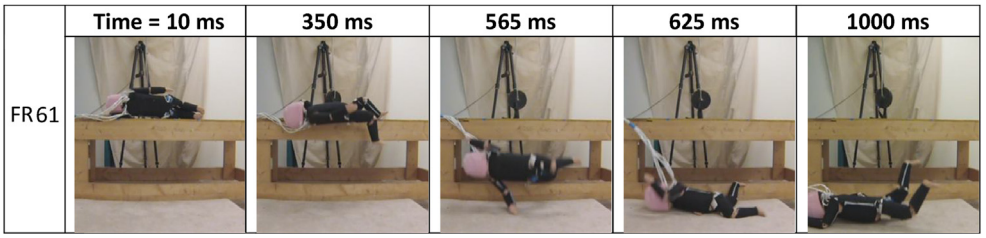

Fig. 6. Video frame sequences of the FR61 (24 in) bed fall onto the padded carpet surface at corresponding time intervals.

The SBDS body map image, showing four views (anterior, posterior, left lateral and right lateral), illustrates the ATD to floor surface impact locations (Fig. 5) for the FF91 bed fall (Fig. 4). Secondary impact following rebound was not evaluated.

3.1.3. Facing rearward – 61 cm bed height (FR61)

The initial ATD position was facing rearward (FR) away from the edge of the bed such that the longitudinal (mid-sagittal plane) axis of the body was parallel with the ground (10 ms, Fig. 6). Subsequent to actuator-ATD contact, the ATD rolled longitudinally rearwards about the edge of the bed surface (350 ms, Fig. 6). During the free fall to the floor, the ATD continued to rotate about its longitudinal axis. The right arm was outstretched and leading the ATD, followed by the legs and head which slightly trailed just prior to impact (565 ms, Fig. 6). The ATD impacted the floor surface in a right anterior aspect with the right arm impacted the floor initially, (the right lower arm was impinged between the chest and floor) followed by the legs, torso and right frontal region of the head (625 ms, Fig. 6). Following the initial impact with the floor, the ATD rebounded upward off the floor before finally coming to rest (1000 ms, Fig. 6).

The SBDS body map image, showing four views (anterior, posterior, left lateral and right lateral), highlighting highlights the ATD to floor surface impact locations (Fig. 7) for the FR61 bed fall as shown in (Fig. 6). Since we were primarily concerned with the initial impact event, data associated with the secondary impact following rebound was not evaluated.

3.1.4. Facing rearward – 91 cm bed height (FR91)

The ATD initial position was facing rearward (FR) such that the longitudinal (mid-sagittal plane) axis of the body was parallel with the floor (10 ms, Fig. 8). Subsequent to actuator-ATD contact, the ATD rolled longitudinally rearward about the edge of the bed surface (350 ms, Fig. 8). During the free fall to the floor, the ATD continued to rotate about its longitudinal axis. The right arm was outstretched leading the ATD with the legs following. The head slightly trailed the legs just prior to impact (700 ms, Fig. 8). The anterior surface of the ATD impacted the floor with the right arm initially, followed by the legs, torso and right frontal region of the head (770 ms, Fig. 8). Following the initial impact with the floor, the ATD rebounded upward off the floor before coming to rest (1000 ms, Fig. 8).

The SBDS body map image, showing four views (anterior, posterior, left lateral and right lateral), illustrates the ATD to floor surface impact locations (Fig. 9) for the FR91 bed fall (Fig. 8). Since we were primarily concerned with the initial impact event, data associated with the secondary impact following rebound was not evaluated.

3.2. Contact forces

The mean peak impact force for the head (2631 N ± 100), anterior torso (1990 N ± 63), right upper leg (2006 N ± 293) and left lower leg (907 N ± 167) were the highest in the FR91 falls. The

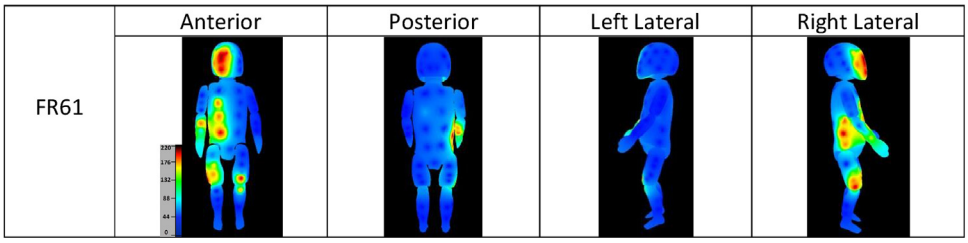

Fig. 7. Representative SBDS body map image corresponding to the FR61 (24 in) bed fall illustrating body regions of impact. Colors and intensity vary depending on level of force imparted to specific regions during the fall event. (For interpretation of the references to color in this figure legend, the reader is referred to the web version of the article.)

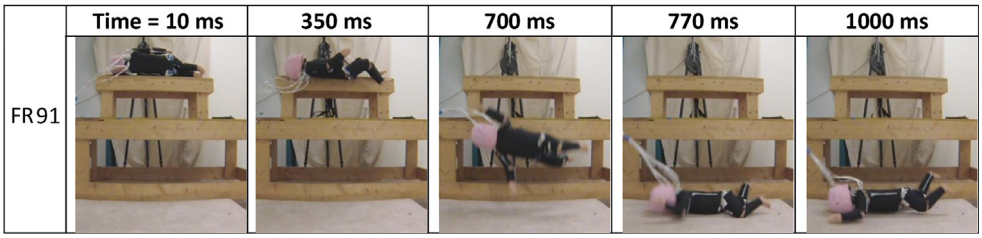

Fig. 8. Video frame sequences of FR91 (36 in) bed fall onto the padded carpet surface at corresponding time intervals.

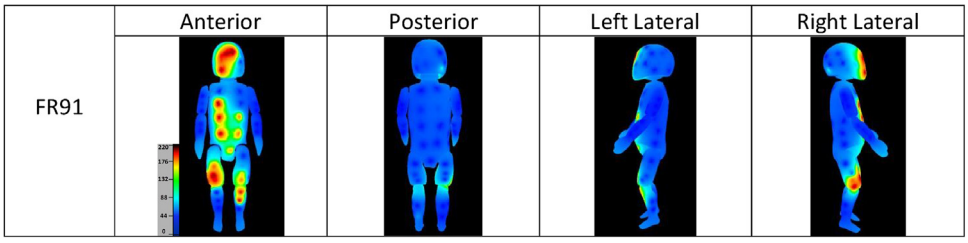

Fig. 9. Representative SBDS body map image corresponding to FR91 (36 in) bed fall illustrating body regions of impact. Color and intensity vary depending on the level of force imparted to specific regions during the fall event. (For interpretation of the references to color in this figure legend, the reader is referred to the web version of the article.)

mean peak impact force for the posterior torso (1945 N ± 146) and left upper arm (1598 N ± 118) were the highest in the FF91 falls. The mean peak impact force for the left upper leg (1249 N ± 158) was the highest in the FF61 falls. The lowest mean peak impact force to the head (2045 N ± 254) occurred in the FF61 falls (Table 3).

Table 3
Mean peak contact force (N) for each body region in various fall scenarios ($n = 5$ trials).

Body region	FF61	FR61	FF91	FR91
Head	2045* (± 254)	2223 (± 112)	2510 (± 179)	**2631* (± 100)**
Anterior Torso	624* (± 137)	912* (± 99)	12 (± 2)	**1990* (± 263)**
Posterior Torso	606* (± 70)	944* (± 192)	**1945 (± 146)**	20 (± 6)
Left Upper Arm	1583*(± 112)	18* (± 3)	**1598 (± 118)**	15 (± 4)
Right Upper Arm	15* (± 2)	11* (± 1)	14 (± 4)	16 (± 7)
Left Lower Arm	18* (± 4)	16* (± 3)	**68 (± 73)**	15 (± 4)
Right Lower Arm	44* (± 37)	**850* (± 115)**	10 (± 3)	11 (± 5)
Left Upper Leg	**1249* (± 158)**	336* (± 149)	424 (± 155)	399 (± 173)
Right Upper Leg	16* (± 2)	1371* (± 194)	15 (± 2)	**2006 (± 293)**
Left Lower Leg	184* (± 67)	322* (± 202)	17 (± 2)	**907 (± 167)**
Right Lower Leg	12* (± 4)	**21* (± 15)**	12 (± 3)	17 (± 7)

Bolded cells indicate maximum mean peak forces (± SD) for each body region comparing all fall scenarios.
↓ – represents recorded forces that were below the established threshold of 5% of ATD body weight.
* – represents significant difference between designate cell and all other fall scenarios in the same body region.
‡ – represents significant differences between designate cell and all other surfaces in the same body region.

The highest levels of force were recorded on the head in all falls compared to other body regions. Across all falls, maximum recorded forces were to the head in FR91 falls. Since injuries to the head typically have the greatest consequences, we focused our analysis on forces imparted to the head relative to fall height and initial ATD position. Head forces differed significantly across falls of varying fall height and initial position, $F(3,16) = 18.46$, $p < 0.001$, $\omega = 0.88$. Both main effects of height and initial position for head impact force were statistically significant, indicating that head impact force differed between 61 cm and 91 cm falls, $F(1,16) = 49.42$, $p < 0.001$, $\omega = 0.83$, and between falls with a forward facing and rearward facing initial position, $F(1,16) = 5.776$, $p < 0.05$, $\omega = 0.28$. The interaction effect of height and position was not significant, $F(1,16) = 0.21$, $p > 0.05$, $\omega = 0.51$, indicating that head impact force measured for a certain fall height was not influenced by ATD initial position. Post hoc Tukey's HSD tests indicated that head impact forces generated by the 61 cm fall heights were significantly different from those in the 91 cm fall heights for both initial conditions ($p < 0.05$). However, the head impact forces generated for different initial positions for the same height did not differ significantly ($p > 0.05$).

3.3. Potential bruising regions – cumulative contact maps

To assess the highest potential for bruising, image maps of each fall scenario were generated representing the maximum recorded force for each sensor across 5 trials. Thus, these maps provide a cumulative representation of contact for each fall scenario.

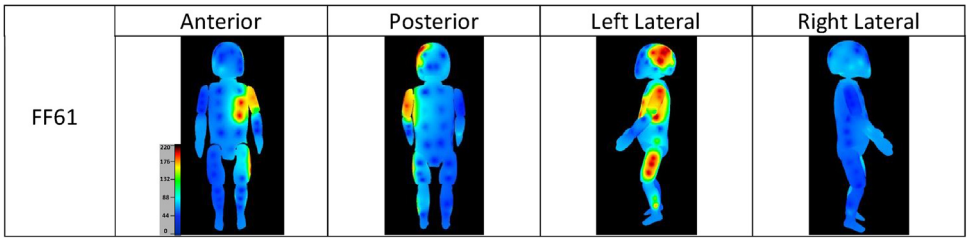

Fig. 10. Cumulative contact regions across 5 trials as recorded by the SBDS for the FF61 fall scenario. The body map images show the anterior, posterior, left lateral and right lateral aspects of the ATD. The colors and intensities vary dependent on level of force (N) imparted to specific regions during the fall event. (For interpretation of the references to color in this figure legend, the reader is referred to the web version of the article.)

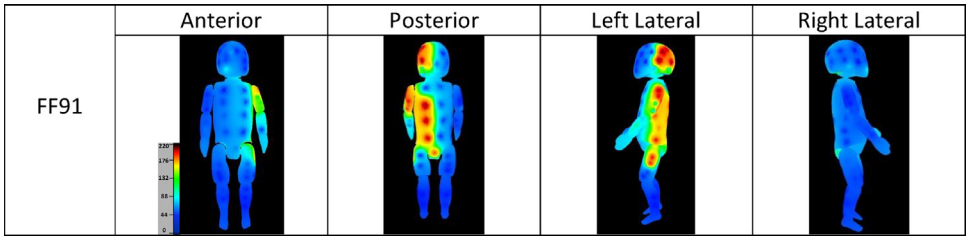

Fig. 11. Cumulative contact regions across 5 trials as recorded by the SBDS for the FF91 fall scenario. The body map images show the anterior, posterior, left lateral and right lateral aspects of the ATD. The colors and intensities vary dependent on level of force (N) imparted to specific regions during the fall event. (For interpretation of the references to color in this figure legend, the reader is referred to the web version of the article.)

3.3.1. Facing forward – 61 cm and 91 cm bed height

The ATD cumulative contact maps differ for 61 cm (Fig. 10) and 91 cm (Fig. 11) FF falls. For the FF61 falls (Fig. 10), the left parietal region of the head, left upper arm and left upper leg reflect the majority of contact forces with the impact surface. The left upper arm was trapped between the chest and floor, therefore contact between the medial aspect of the left upper arm and left lateral region of the chest was observed. Other than the left upper arm and left lateral chest, the anterior plane, posterior plane and right lateral plane of the ATD recorded no contact with the floor.

In comparison, the FF91 falls highlight impact on the left lateral posterior regions of the head, torso and left upper arm and leg, and showed no contact in the anterior and right lateral planes of the ATD (Fig. 11). There was also contact to the occipital region of the head.

3.3.2. Facing rearward – 61 cm and 91 cm bed height

The ATD cumulative contact maps differ for the 61 cm (Fig. 12) and 91 cm (Fig. 13) FR falls. For the FR61 falls (Fig. 12), contact is primarily to the right frontal region of the head and torso, and right upper leg. The right lower arm contact was from impingement between the chest and floor surface. No contact was recorded on the posterior plane and left lateral plane of the ATD.

In comparison, the FR91 falls highlight impact on the anterior plane of the ATD and show no contact in the posterior and left lateral planes. There was contact to the frontal region of the head, anterior torso, and anterior regions of the right and left upper legs and left lower leg (Fig. 13).

4. Discussion

4.1. Dynamics

Leading up to impact, fall dynamics were similar in falls from different heights when initial position was maintained. However, in the higher falls (91 cm), the larger fall distance allowed the ATD to rotate longitudinally for a longer time period prior to impact as compared to the 61 cm falls. These findings are similar to those of Thompson et al. [11] who conducted a parametric sensitivity analysis using a validated computer model to simulate a bed fall of a CRABI 12-month old ATD. The Thompson model was used to investigate the influence of altering fall parameters on injury outcome measures. Thompson found that increasing or decreasing bed height had an influence on fall dynamics and impact orientation.

Fall dynamics of FF61 falls closely resemble the dynamics of Thompson et al. [12] simulating bed falls from 61 cm (24 in) high, using a CRABI – 12-month-old. An initial side lying position similar to our facing forward position was used. Thompson's reported fall dynamics closely resembling our experiments with rotation about

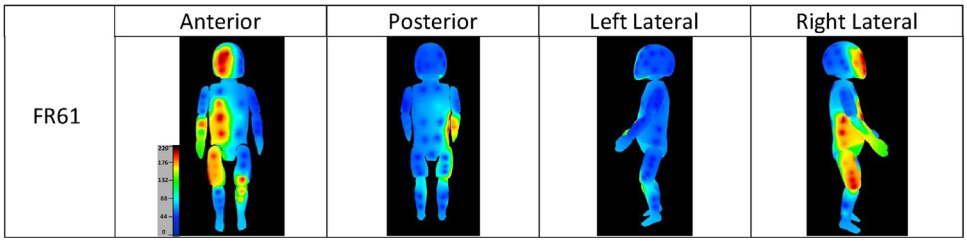

Fig. 12. Cumulative contact regions across 5 trials as recorded by the SBDS for the FR61 fall scenario. The body map images show the anterior, posterior, left lateral and right lateral aspects of the ATD. The colors and intensities vary dependent on level of force (N) imparted to specific regions during the fall event. (For interpretation of the references to color in this figure legend, the reader is referred to the web version of the article.)

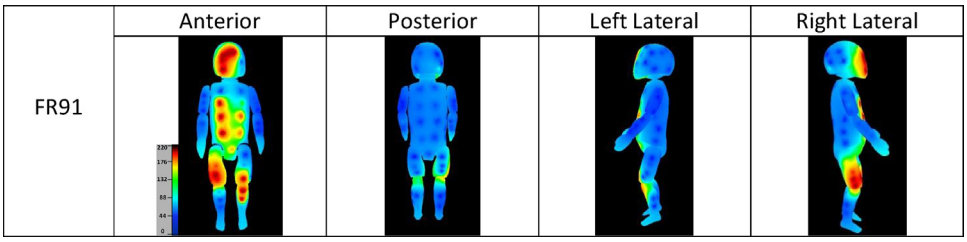

Fig. 13. Cumulative contact regions across 5 trials as recorded by the SBDS for the FR91 fall scenario. The body map images show the anterior, posterior, left lateral and right lateral aspects of the ATD. The colors and intensities vary dependent on level of force (N) imparted to specific regions during the fall event. (For interpretation of the references to color in this figure legend, the reader is referred to the web version of the article.)

the longitudinal axis while free falling to the ground, simultaneously impacting with the head and left shoulder.

Bertocci et al. [13] simulated bed falls from a 68 cm (27 in) high horizontal surface using a Hybrid II 3-year old ATD. The initial position was a side lying position similar to our facing forward position. Reported fall dynamics were similar to ours prior to impact, however, possibly because of the ATD size disparity; their findings indicated initial leg or pelvis impact, whereas the ATD shoulder and head initially contacted the surface in our experiments.

Fall dynamics differed when comparing falls with varying initial position (FF and FR) at the same fall height; the ATD had greater longitudinal rotation in the FR falls compared to the FF falls. The approximate total longitudinal rotation of the ATD from initial position until moment of impact with the floor for FF falls was ≈180° and ≈225° at 61 cm and 91 cm heights, respectively. Alternatively the approximate total longitudinal rotation of the ATD from initial position until impact with the floor for FR falls was ≈225° and ≈270° at 61 cm and 91 cm heights, respectively. The ATD's leg position influenced the ATD's rotational resistance at push off. In the FF position, the ATD's legs are positioned facing toward the edge of the bed surface, whereas in the FR falls, the ATD's legs are positioned facing away from the edge of the bed surface. Once the FR fall was initiated the ATD began rotating about a longitudinal axis that passes within the ATD torso. Conversely, in FF falls the ATD rotated about a longitudinal axis that was located between the torso and knees. This difference in rotational axis position led to differing rotational resistance, which can be characterized by the effective moment of inertia. Moment of inertia can be thought of as resistance to rotation, and increases as limbs (and their associated mass) are extended away from the body. The moment of inertia about the rotational axis in FF falls is greater than that in FR falls because of the legs influence on the rotation before the ATD leaves the bed surface. The higher moment of inertia associated with increased rotational resistance tends to decrease speed of rotation. Thus, the total longitudinal rotation from push off to impact was less for the FF falls than FR falls.

4.2. Forces

The mean peak head impact force (2631 N ± 100) was the highest in 91 cm FR falls and the lowest mean peak head impact force (2045 N ± 254) occurred in the 61 cm FF falls.

Several studies have investigated head injury risk in pediatric falls using varying representative ages of ATD's. Thompson et al. [12] conducted bed fall experiments from a 61 cm (24 in) high horizontal surface using a CRABI – 12 month old falling from a side lying position (similar to our FF initial position) onto five different impact surfaces. They reported average linear head acceleration of 85 g for falls onto padded carpet. Using a CRABI-12 head mass of 2.6 kg (5.8 lb), this results in an estimated head impact force of 2170 N (±140) for falls onto padded carpet over wood – similar to that measured in our experiments.

Coats et al. [14] developed an instrumented infant (1.5 month old) surrogate to measure head impact forces and angular accelerations associated with low-height falls. The surrogate was dropped from a supine position with arms and legs extended to the sides of the body from heights between 0.3 and 0.9 m (12 in and 36 in) onto three impact surfaces - mattress, carpet pad, and concrete. The peak head impact force in the fall experiments was approximately 650 N for the 0.6 m (24 in) falls and 1000 N for the 0.9 m (36 in) falls onto carpet surface. Ibrahim et al. [15] simulated falls using an 18-month-old surrogate that was suspended in a supine position and allowed to free fall from heights of 0.3 m, 0.6 m and 0.9 m (12 in, 24 in and 36 in) onto carpet pad and concrete. Peak estimated head impact force was approximately 3715 N (± 850) and 4570 N (± 285) for the 0.6 m and 0.9 m (24 in and 36 in) falls onto carpet pad, respectively. Bertocci et al. [13] conducted bed falls from a 0.68 m (27 in) high horizontal surface using a Hybrid II 3-year old ATD with a similar initial position as compared to our FF falls. The falls were conducted onto four impact surfaces including wood, padded carpet, linoleum and playground-foam. Results indicated linear head accelerations of approximately 160 g (±60) for falls onto padded carpet. Based upon an ATD head mass of 2.7 kg (6 lb), these head accelerations yield an estimated head impact force of 4237 N for falls onto padded carpet over wood.

The head impact forces measured in our fall experiments in comparison to the studies described above are summarized in Table 4. Head impact forces associated with 61 cm FF falls in our experiments are in reasonable agreement with those reported by Thompson et al. [12] for falls using the same ATD, initial position and fall height. The head impact forces in Coats et al. [14] are lower than our findings for a few reasons. Coats used a custom designed ATD representing an infant which is younger in age (1.5 months) than ours (12 months) and has a neck design that is less stiff than the CRABI 12 ATD neck. In addition to the reduced neck stiffness, the lighter mass of the head and different initial position (supine) in Coats's study are likely responsible for head forces that differ from those in our study. Conversely, head impact forces from the Ibrahim et al. [15] and Bertocci et al. [13] studies are higher than our findings mainly because of the difference in ATD mass. Ibrahim used a custom designed ATD which is older in age (18 months), in addition to a different initial position (supine free fall). The Bertocci et al. [13] study also used an older ATD (Hybrid II 3-year-old), which has greater mass (13.6 kg, 30 lb) versus ours (9.1 kg, 20 lb), likely accounting for greater head forces. It should be noted that the head forces for the Thompson et al. [12] and Bertocci et al. [13] studies were calculated from measured head accelerations and head mass, and are therefore estimates of head impact forces.

4.3. Contact regions

In assessing body regions of impact during simulated falls, it is important to compare ATD morphology/geometric shape to that of an infant's morphology. The CRABI-12 ATD morphology (external shape/geometry) may vary somewhat from that of a 12-month-old

Table 4
Comparison of head impact forces, ATD properties and initial conditions for various fall studies.

	Our Study	Thompson et al. [12]	Coats et al. [14]	Ibrahim et al. [15]	Bertocci et al. [13]
Head force (N)– 61 cm Fall	2045–2223	2170[a]	650	3715	4237[a]
Head force (N) – 91 cm Fall	2510–2631	–	1000	4570	–
ATD age	12 month	12 month	1.5 month	18 month	36 month
Head contact region	Frontal, Parietal, Occiput	Parietal[b]	Occiput	Occiput	Occiput[b]
Head mass (kg)	2.6	2.6	2.1	2.3	2.7
Fall type, ATD orientation	Bed fall, side lying, FF, FR	Bed fall, side lying, FF	Supine, free fall	Supine, free fall	Bed fall, side lying, FF

[a] Force calculated from measured acceleration and head mass.
[b] Assumed to be to the posterior aspect of the head but not specified in study.

50th percentile infant. For example, the ATD morphology does not replicate soft tissue of the buttocks region; instead in our study, the proximal posterior upper leg region of the ATD represents the buttocks. The ATD head morphology provides a reasonable replica of a 12-month child (Fig. 14) but does not include ears, nose, lips and orbital region of the eyes as individual features. Also, the ATD head morphology does not represent the caudal most aspects of the occipital region or the mandible. Thus, it was not possible to measure and record impact to these regions. Also, we do not have sensors on the neck region of the ATD given its construction (segmented rubber and aluminum). Despite these differences, the CRABI-12 provides a reasonable representation of the overall head geometry.

In any given fall scenario we recorded a commonality of contact within at most two planes (across all trials; $n = 20$). Additionally, a consistent pattern emerged; the majority of contact regions and greater forces were recorded in one plane, with fewer regions of contact and decreased force exhibited in the second adjoining plane. Additionally, our findings suggest no possibility of bruising (no contact recorded) in the two planes opposite to the impact planes for each fall scenario (Table 5). It is pertinent that the design of the boundaries/extremities of the individual sensors that make up the SBDS are not explicitly directed by the body planes. That is, individual sensors cross over multiple planes and therefore could indicate impact in more than one plane even though the acting force was not directed to multiple planes. Additionally, articulation

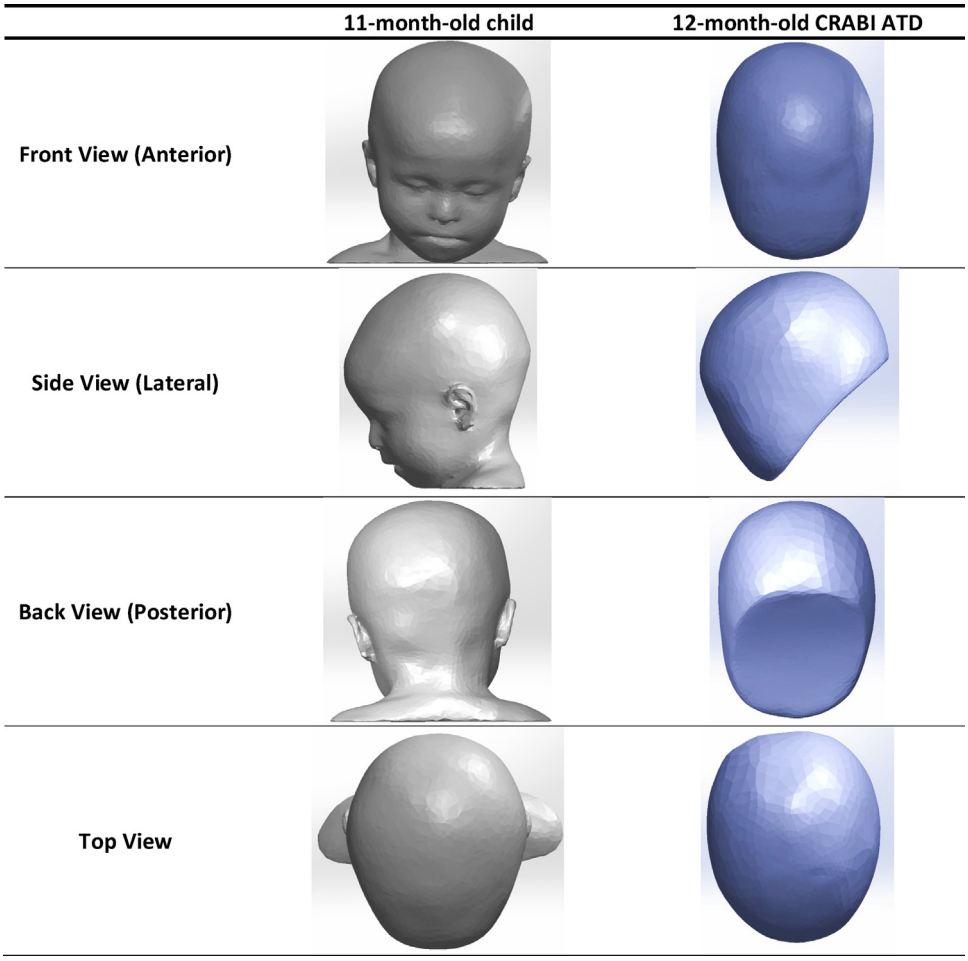

Fig. 14. Comparative views of an 11-month-old child (3D reconstruction of CT imaging) and the 12-month-old CRABI ATD highlighting morphological differences in head profile. (For interpretation of the references to color in this figure legend, the reader is referred to the web version of the article.)

Table 5
Overview of body planes with and without contact with the impact surface as observed in all conducted experimental falls.

Fall Type	Plane with contact	Plane without contact
FF 61	L Anterior L Lateral	Posterior R Lateral
FF 91	L Posterior L Lateral	Anterior R Lateral
FR 61	Anterior R Lateral	Posterior L Lateral
FR 91	Anterior R Lateral	Posterior L Lateral

Note: Individual sensor placement is not segregated along planes – some sensors have coverage on multiple planes.

of the extremities following fall initiation and during impact with the surface could influence ATD regions of impact and consequently the planes of impact.

When assessing children with bruises, the location and pattern (constellation of individual bruises throughout the body) of bruising is especially important when attempting to delineate accidental from abusive trauma. Several studies have investigated the distinction between bruising patterns in abused children versus those seen in accidental circumstances. Maguire et al. [16] reviewed studies that noted bruises resulting from accidental trauma occurred predominantly on the anterior regions of the body, over bony prominences and were correlated to the child's level of independent mobility. In abused children the bruises tended to be larger and the most common sites were the face, neck, ear, head, trunk, buttocks, and arms. Kemp et al. [7] discovered abused children were significantly more likely to have bruising than those where abuse was ruled out. Abused children also had significantly more bruises, bruising sites and clustering of bruises. Bruising to the left ear, cheeks, neck, trunk, front of thighs, upper arms, buttocks and genitalia were found significantly more frequently in abused children, than when abuse was ruled out. Pierce, Kaczor et al. [6] studied the skin findings (bruises, lacerations, etc.) of children ages 0–4 years that were admitted to the pediatric intensive care unit; differences in body regions with bruising were identified for children with abusive versus accidental trauma. The face, cheek, scalp, head, and legs had bruising in patients with abusive and accidental trauma; these regions did not delineate between accident and abuse. However, bruising to the ear, neck, hands, right arm, chest and buttocks regions were predictive of abuse. Bruising to the genitourinary area and hip occurred only in patients with abusive trauma.

The impact regions recorded in our testing compared to the bruising locations found on children from described relevant studies are summarized in Table 6.

Collectively across all fall scenarios we predominantly found impact to the head, torso, left upper arm, right lower arm, left and right upper legs and left lower leg. Compared to previous clinical studies describing bruising locations for a range of accident types, the head and posterior torso were found to be common regions of bruising. However, Kemp et al. [7] and Maguire et al. [16] did not report detailed fall description, mechanism or injury causation which limits direct comparisons as our experimental findings in Table 6 are specific to bed fall scenarios.

In our previous study, where the bruising detection system was used to investigate rearward falls from standing [17], there are differences in potential bruising pattern compared to this study. For the rearward falls from standing [17], the posterior plane was the only plane of contact and included the occipital region of the head, posterior torso, posterior legs and posterior upper arms. However in our bed fall experiments, we recorded 2 planes of contact with varying degrees impact to the head, torso, arms and legs region dependent upon fall characteristics (i.e. fall height and initial position). In combination, these studies indicate that different fall types lead to different potential bruising locations on the body. Differing potential bruising patterns across fall scenarios suggest that determining compatibility between a child's injuries and stated fall history is critical in the injury assessment process, and will be dependent upon fall characteristics. This finding further emphasizes the need to obtain detailed histories when interviewing caregivers.

5. Limitations

The CRABI-12 ATD was primarily designed for approximating and quantifying a child's response to a high energy motor vehicle crash, thus use of the ATD in lower deceleration events such as falls should be interpreted in light of biofidelity limitations. For example, the neck is stiffer than a child's with limited range of motion designed for frontal impacts having little or no out of plane motion. Rubber bushings at the attachment of limbs to the ATD torso are intended to provide joint range of motion and joint resistance to motion at the hips and shoulders; however, they fall short of infant joint biofidelity. In addition, shoulders, elbows, hips, and knees of the ATD are limited to motion primarily in the sagittal plane. Biofidelity of the soft tissue is another limitation of the CRABI ATD, and thus the SBDS. The ATD surrogate “soft tissue” consists of a heat cured vinyl plastisol that is layered with urethane foam between the outer and inner layers. The plastisol is compliant and molded to mimic the body contours representing “soft tissue”.

Table 6
Comparison of bruising locations for various studies.

	Our study	Kemp et al. [7]	Maguire et al. [16]	Pierce et al. [6]
Regions of abusive bruising	–	Head, cheek, ear, neck, trunk, upper arms, front of thighs,	Head including face, front of body, ear, neck, trunk, arms, buttocks	All regions including torso, ear and neck
Regions of Accidental Bruising	[a]Head, Torso, L upper arm, R lower arm, L & R upper leg, L lower leg	Head, rear trunk	Head, forehead, back, abdomen, forearms, hands, buttocks, knees, shins, foot	All regions excluding torso, ear and neck

[a] Recorded impact locations that could represent potential bruising locations specific to bed falls.

SBDS sensor-measured forces are proportional to the stiffness of the underlying ATD surrogate soft tissue; therefore soft tissue biofidelity greatly influences the measured forces. However, our primary goal was to determine points of contact during various injurious events and secondarily to assess relative levels of force imparted to different regions of the body. Thus, biofidelic limitations of the surrogate soft tissue do not prevent us from meeting these goals.

The occurrence of a bruise for a given application of force varies from person to person based on many contributing factors that affect bruise development. Extrinsic factors such as the amount of force applied, rate of force application, and distribution of the force over larger/smaller areas are parameters that can affect the presence or absence of a bruise. Additionally, intrinsic factors related to the physiological and anatomical structures, such as architecture of the skin, soft tissue thickness, toughness of skin, fat content, vessel fragility, and presence and depth of underlying bone add to the complexity of this physiological event. Variables such as blood platelet levels, systemic blood pressure, vascular diseases and vasoactive or anticoagulant drug use in addition to nutritional and allergy related disorders can have a great influence on the presence, absence and variability in intensity of bruise. This implies that the minimum load to cause bruising, the "bruising threshold", varies across individuals. However it can be said with some degree of certainty that larger forces are associated with a greater potential for bruising. So instead of definitively asserting the presence of a bruise, we envision our device to be used as an investigative tool to determine potential bruising locations occurring within a body region under specific loading conditions.

Variations in impact surfaces may influence fall dynamics and thus contact locations. Variations in initial fall position and fall height for the ATD may lead to differing results. Additionally, children may alter their position in bed over the course of their sleep cycle, necessitating the evaluation of multiple initial fall positions. Active muscle response and protective reflexes during a fall are not accounted for in our ATD model. However, children ≤ 1 year would exhibit limited muscle response in a fall. Moreover, a sleeping child would not tend to activate their muscles during a fall. Also, the surrogate bruising detection system (SBDS) consisting of the ATD and the overlaying sensing system, could be improved by either improving the biofidelity of the ATD to better represent a child and/or improving sensor density so as to record contact location data with greater detail.

These limitations must be considered when using the ATD-adapted force sensing skin to assess bruising potential in falls and when interpreting associated findings.

6. Conclusions

In this study a surrogate bruising detection system adapted to an ATD representing a 12-month-old was used to investigate potential bruising locations (as indicated by contact during impact) associated with bed falls from varying heights and initial positions. Across all trials, primary contact occurred on one plane of the ATD body, with secondary contact occurring only on adjoining planes; no contact was recorded on planes opposite those with recorded contact. Regions of contact were found to differ with varying fall heights and initial positions. Fall height and initial position also influenced maximum head impact force. Our findings related to planes of potential bruising can be used when attempting to distinguish between accident and abuse in the presence of a bed fall history. However, it should be noted that individual histories of bed falls must be carefully evaluated to determine the veracity of the history. Experimental findings from our study cannot be generalized across all bed falls, but should be used as a guide when conducting a biomechanical assessment. Also, not all recorded regions of contact translate to a bruise but rather a potential for bruising. While many extrinsic and intrinsic factors determine whether bruising will occur on impact, documentation of potential bruising locations based upon recorded contact to individual body regions is a first step toward understanding bruising patterns that may result from a bed fall. This knowledge can potentially aid in delineating bruising patterns associated with an accidental bed fall versus that of a falsely reported bed fall.

Acknowledgements

This study was funded by the National Institute of Justice (Grant no. # 2008-DD-BX-K311) and by the Office of Juvenile Justice and Delinquency Prevention (Grant no. # 2009-DD-BX-0086), Office of Justice Programs, US Department of Justice. Points of view or opinions expressed herein are those of the authors and do not necessarily represent the official position or policies of the US Department of Justice.

We would like to acknowledge Dr. Angela Thompson for her assistance in our statistical assessment of the data and help in converting CT image files to a 3D solid model. Additionally, post-mortem CT data was provided courtesy of the University of New Mexico Radiology-Pathology Center for Forensic Imaging, supported by National Institute of Justice Grant 2010-DN-BX-K205.

References

[1] DHHS, Child Maltreatment 2015, U.S. Department of Health and Human Services, Administration for Children and Families, Washington, DC, 2015.
[2] R. Alexander, L. Crabbe, Y. Sato, W. Smith, T. Bennett, Serial abuse in children who are shaken, Arch. Pediatr. Adolesc. Med. 144 (1) (1990) 58–60.
[3] C. Jenny, K.P. Hymel, A. Ritzen, S.E. Reinert, T.C. Hay, Analysis of missed cases of abusive head trauma, JAMA 281 (7) (1999) 621–626.
[4] S. Maguire, M.K. Mann, J. Sibert, A. Kemp, Are there patterns of bruising in childhood which are diagnostic or suggestive of abuse? A systematic review, Arch. Dis. Child. 90 (2) (2005) 182–186.
[5] F.D. Dunstan, Z.E. Guildea, K. Kontos, A.M. Kemp, J.R. Sibert, A scoring system for bruise patterns: a tool for identifying abuse, Arch. Dis. Child. 86 (5) (2002) 330–333.
[6] M.C. Pierce, K. Kaczor, S. Aldridge, J. O'Flynn, D.J. Lorenz, Bruising characteristics discriminating physical child abuse from accidental trauma, Pediatrics 125 (1) (2010) 67–74.
[7] A.M. Kemp, S.A. Maguire, D. Nuttall, P. Collins, F. Dunstan, Bruising in children who are assessed for suspected physical abuse, Arch. Dis. Child. 99 (2) (2014) 108–113.
[8] K. Nayak, N. Spencer, M. Shenoy, J. Rubithon, N. Coad, S. Logan, How useful is the presence of petechiae in distinguishing non-accidental from accidental injury? Child Abuse Neglect 30 (5) (2006) 549–555.
[9] K. Nayak, N. Spencer, Design and development of a force sensing skin adapted to a child surrogate to identify potential bruising locations, Technology 02 (01) (2014) 49–54.
[10] K. Nayak, Soft Tissue Impact Assessment Device and System, (2008) .
[11] A. Thompson, G. Bertocci, Pediatric bed fall computer simulation model: parametric sensitivity analysis, Med Eng Phys 36 (1) (2014) 110–118.
[12] A. Thompson, G. Bertocci, M.C. Pierce, Assessment of injury potential in pediatric bed fall experiments using an anthropomorphic test device, Acc. Anal. Prev. 50 (2013) 16–24.
[13] G.E. Bertocci, M.C. Pierce, E. Deemer, F. Aguel, J.E. Janosky, E. Vogeley, Using test dummy experiments to investigate pediatric injury risk in simulated short-distance falls, Arch. Pediatr. Adolesc. Med. 157 (5) (2003) 480–486.
[14] B. Coats, S.S. Margulies, Potential for head injuries in infants from low-height falls, J. Neurosurg. Pediatrics 2 (5) (2008) 321–330.
[15] N.G. Ibrahim, S.S. Margulies, Biomechanics of the toddler head during low-height falls: an anthropomorphic dummy analysis, J. Neurosurg. Pediatrics 6 (1) (2010) 57–68.
[16] S. Maguire, M. Mann, Systematic reviews of bruising in relation to child abuse-what have we learnt: an overview of review updates, Evid. Based Child Health 8 (2) (2013) 255–263.
[17] R. Dsouza, G. Bertocci, Impact sites representing potential bruising locations associated with rearward falls in children, Forensic Sci. Int. 261 (2016) 129–136.